The Astrophysical Journal, 633:953–966, 2005 November 10

ULTRAVIOLET RADIATION INSIDE INTERSTELLAR GRAIN AGGREGATES. II. FIELD DEPOLARIZATION

Rosalba Saija
Dipartimento di Fisica della Materia e Tecnologie Fisiche Avanzate, Università di Messina, Salita Sperone 31, 98166 Messina, Italy

Cesare Cecchi-Pestellini
Osservatorio Astronomico di Cagliari, Loc. Poggio dei Pini, Strada 54, 09012 Capoterra, Italy

Maria Antonia Iatì, Arianna Giusto, Ferdinando Borghese, and Paolo Denti
Dipartimento di Fisica della Materia e Tecnologie Fisiche Avanzate, Università di Messina, Salita Sperone 31, 98166 Messina, Italy; iati@ortica.unime.it

and

Santi Aiello
Dipartimento di Astronomia e Scienza dello Spazio, Università di Firenze, Largo Enrico Fermi 5, 50125 Florence, Italy
Received 2005 January 21; accepted 2005 July 19

ABSTRACT

We study the polarization of the UV light within the cavities of interstellar grain aggregates modeled as homogeneous spheres containing several spherical voids. The incident field is a linearly polarized plane wave. We found that field depolarization occurs in all examined cases so that the field within the cavities has the features of an elliptically polarized wave. The depolarization of the field does not depend on the material of the grains but on the geometry of the problem only. The implications of this result for the interstellar photochemistry are briefly discussed.

Subject headings: dust, extinction — radiative transfer

Online material: color figures

1. INTRODUCTION

Planetary systems such as our own are believed to form from the collapse of an interstellar dense cloud composed of molecular gas and submicrometer sized grains. In such clouds the temperatures are lower than 50 K, and all but the most volatile species condense onto grains, coating them with a thin layer of ice (Whittet 1992). Interstellar ice consists primarily of water ice, but carbon- and nitrogen-bearing molecules are also present (Gibb et al. 2004). Laboratory studies and astronomical observations indicate that radiation processing of such ices leads to complex organic compounds (Gerakines et al. 1996).

On the basis of the ubiquitous presence of disks around young stars as well as theoretical models, it is generally accepted that the primordial solar nebula was composed of gas and mutually colliding dust grains, eventually giving rise to a collection of bodies ranging from small grains to meteorites, and later (within a few tens of million years) to planets (e.g., Lissauer 1993). Analysis of cometary dust grains show that these grains appear to consist of units, monomers, whose sizes are tens of nm. Monomers can aggregate into fluffy particles with typical sizes 0.1–10 μm. Comets are primitive small bodies that are believed to contain interstellar and circumstellar silicates and other presolar components, for example, organic compounds (Wooden et al. 1999). This suggestion is substantiated by the identification of interstellar subgrains, as evidenced by their isotopic composition, in interplanetary dust particles that provide a spectral match to astronomical amorphous silicates (Bradley et al. 1999) and to the 2175 Å extinction feature ubiquitous in the interstellar medium (Bradley et al. 2005).

The formation of dust aggregates by coagulation has been discussed extensively in the literature (e.g., Dominik & Tielens 1997). The timescale for the accretion of volatiles is much faster than that of cluster aggregation (Draine 1985), suggesting that coagulation will occur when dust grains have already acquired an ice mantle. During the process, substantial amounts of vacuum might be incorporated in the conglomerate, producing cavities and voids partly filled with molecular condensate. The extent of fluffiness depends on the particular hosting astronomical region, and it is likely to be quite variable. Duley (2000) noted that the chemistry in the interiors of grain aggregates offers a completely new perspective with respect to the one in action on grain surfaces. It is this internal volume that leads, in the physical conditions of the primordial solar nebula, to the possibility of a peculiar terrestrial type chemistry induced by cosmic rays, X-rays, and ultraviolet (UV) radiation (Cecchi-Pestellini et al. 2004). Indeed, the observations of young solar-type stars (having an age of less than 10 million years) in the Milky Way, considered to represent the early Sun, as well as meteoritic data, show that the early Sun was much more active than it is today (Micela 2002). Thus, the production of complex molecules, including prebiotic and biotic compounds, might then be expected.

The formation yield of complex molecules depends critically on the dose of UV radiation impinging on the molecular material (Gerakines et al. 1996). In an earlier work (Cecchi-Pestellini et al. 2005), we presented a detailed analysis of the electromagnetic field in the interiors of interstellar grain aggregates in terms of energy density distribution. We found that the interiors of grain aggregates are illuminated by a substantial fraction of the incident radiation. The results of this analysis have implications for the photochemistry of icy mixtures trapped in aggregate cavities, in their most general application, and they are relevant for studies of any photochemical process that is proposed to occur inside a dust grain, for example, photoluminescence of irradiated dust grains (Malloci et al. 2004), considered to be the likely mechanism producing the ubiquitous extended red emission (Draine 2003).

In the present work we focus on the polarization properties of the field inside dust aggregate cavities. Our specific purpose is

to show that when linearly polarized waves hit the grain, the field within the cavities undergoes a depolarization. As a result, the field at the internal surface of the cavities acquires the features of a circularly polarized wave. This fact has connections to meteoritics and observed amino acid asymmetries (Cronin & Pizzarello 1997; Jorissen & Cerf 2002).

In § 2 we outline the approach exploited in calculating the electromagnetic field and its polarization inside a compact dust grain aggregate modeled as a sphere containing one or more spherical cavities. Results are presented in § 3. Section 4 contains our conclusions.

2. THEORY

2.1. *The Field*

In this section we present the method for computing the electromagnetic field inside a spherical particle containing one or more spherical inclusions that may be also empty cavities. The theory for the calculation of the field scattered by such a model has been published elsewhere (Borghese et al. 1992, 1994, 2002).

The hosting sphere has radius ρ_0, refractive index n_0, and homogeneous chemical composition. For greater generality the center of the host sphere is chosen to lie at $\boldsymbol{R}_0$, even though in practical calculations we put $\boldsymbol{R}_0 = 0$. The inclusions, labeled by an index α, have radii ρ_α and refractive indexes n_α. The geometry is shown in Figure 1, where for the sake of clarity only one inclusion is depicted. The location of an inclusion is determined by the two polar angles θ_c and ϕ_c, defining the angular location of the center of the cavity, and by the distance of the latter from the center of the hosting sphere, $|\boldsymbol{R}_\alpha|$. In the following, all results will refer to the intercepts of the wave propagation direction with the surface of an embedded cavity, reported in Figure 1 as points B (backward) and F (forward). We partition off the space into three regions: (1) the external region, assumed to be filled by a homogeneous medium with real refractive index n (typically the vacuum); (2) the interstitial region; and (3) the inclusions, which may be voids. We assume that all the fields depend on time through the factor $\exp(-i\omega t)$, which is omitted throughout, and we define the propagation constants in the three regions described above as

$$k = nk_v, \quad k_0 = n_0 k_v, \quad k_\alpha = n_\alpha k_v, \tag{1}$$

where $k_v = \omega/c$ is the propagation constant in vacuo. The incident field is the linearly polarized plane wave

$$\boldsymbol{E}_{I\eta} = E_0 \hat{\boldsymbol{u}}_\eta \exp(i\boldsymbol{k}_I \cdot \boldsymbol{r}_0), \tag{2}$$

where $\boldsymbol{k}_I = k\hat{\boldsymbol{k}}_I$ is the propagation vector, $\boldsymbol{r}_0 = \boldsymbol{r} - \boldsymbol{R}_0$, and $\hat{\boldsymbol{u}}_\eta$ is the unit polarization vector whose index $\eta = 1, 2$ indicates whether the electric field is parallel ($\eta = 1$) or perpendicular ($\eta = 2$) to a fixed plane of reference through $\hat{\boldsymbol{k}}_I$. The incident field and the field within the inclusions are expanded in a series of the vector multipole fields (Rose 1957; Borghese et al. 2002)

$$\begin{aligned} \boldsymbol{J}^{(1)}_{lm}(\boldsymbol{r}_\alpha, k_\alpha) &= j_l(k_\alpha r)\boldsymbol{X}_{lm}(\hat{\boldsymbol{r}}_\alpha), \\ \boldsymbol{J}^{(2)}_{lm}(\boldsymbol{r}_\alpha, k_\alpha) &= \frac{1}{k_\alpha}\nabla \times \boldsymbol{J}^{(1)}_{lm}(\boldsymbol{r}_\alpha, k_\alpha), \end{aligned} \tag{3}$$

that are regular at the origin. In equation (3), $\boldsymbol{r}_\alpha = \boldsymbol{r} - \boldsymbol{R}_\alpha$, j_l are spherical Bessel functions, and $\boldsymbol{X}_{lm}$ are vector spherical harmonics (Jackson 1975). Superscripts 1 and 2 refer to the values of a parity index p that distinguishes magnetic multipoles ($p = 1$) from the electric ones ($p = 2$). The expansion of the scattered field and of the field in the interstitial region requires also the introduction of the multipole fields $\boldsymbol{H}^{(p)}_{lm}(\boldsymbol{r}, K)$ that are identical to the $\boldsymbol{J}$ multipole fields except for the substitution of the Hankel function of the first kind $h_l(Kr)$ in place of the Bessel functions $j_l(Kr)$, where K is the appropriate propagation constant. The $\boldsymbol{H}$ fields satisfy the radiation condition at infinity.

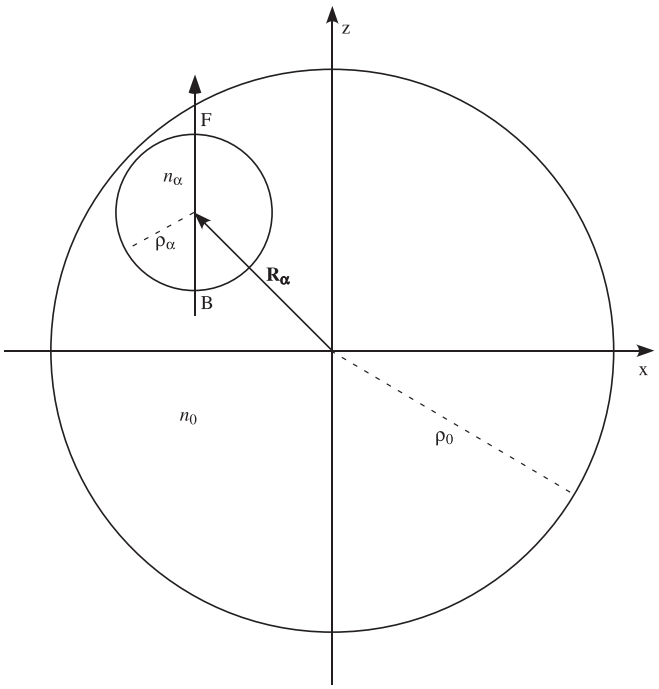

FIG. 1.—Geometry adopted in our calculations. Only one cavity is shown for the sake of clarity.

The field in the external region is the superposition of the incident plane wave and of the field scattered by the target

$$\boldsymbol{E}_{\mathrm{ext}\eta} = \boldsymbol{E}_{I\eta} + \boldsymbol{E}_{S\eta} = E_0 \sum_{plm} \left[\boldsymbol{J}^{(p)}_{lm}(\boldsymbol{r}_0, k) W^{(p)}_{\eta lm} + \boldsymbol{H}^{(p)}_{lm}(\boldsymbol{r}_0, k) A^{(p)}_{\eta lm} \right]. \tag{4}$$

The amplitudes of the scattered multipole fields $A^{(p)}_{\eta lm}$ are labeled by the index η to recall the polarization of the incident field. The multipole amplitudes of the incident field, $W^{(p)}_{\eta lm}$, containing all the information on both the direction of incidence and the polarization are defined as

$$W^{(p)}_{\eta lm} = 4\pi i^{p+l+1} \hat{\boldsymbol{u}}_\eta \cdot \boldsymbol{Z}^{(p)*}_{lm}(\hat{\boldsymbol{k}}_I), \tag{5}$$

where an asterisk denotes complex conjugation and

$$\boldsymbol{Z}^{(1)}_{lm}(\hat{\boldsymbol{k}}) = \boldsymbol{X}_{lm}(\hat{\boldsymbol{k}}), \quad \boldsymbol{Z}^{(2)}_{lm}(\hat{\boldsymbol{k}}) = \boldsymbol{X}_{lm}(\hat{\boldsymbol{k}}) \times \hat{\boldsymbol{k}} \tag{6}$$

are transverse harmonics (Fucile et al. 1997). In the interstitial region, the field is expanded as

$$\boldsymbol{E}_{T\eta} = E_0 \sum_{plm} \left[\sum_\alpha \boldsymbol{H}^{(p)}_{lm}(\boldsymbol{r}_\alpha, k_0) P^{(p)}_{\eta\alpha lm} + \boldsymbol{J}^{(p)}_{lm}(\boldsymbol{r}_0, k_0) P^{(p)}_{\eta 0 lm} \right], \tag{7}$$

whereas the expansion of the field within the αth inclusion is

$$\boldsymbol{E}_{C\eta\alpha} = \sum_{plm} \boldsymbol{J}_{lm}^{(p)}(\boldsymbol{r}_\alpha,\ k_\alpha) C_{\eta\alpha lm}^{(p)}. \tag{8}$$

The unknown amplitudes are determined imposing the customary boundary conditions across the surface of the hosting sphere and across the surface of each inclusion.

Multipole fields have different origins. Using an appropriate addition theorem (Borghese et al. 1980, 2002), we can refer all the multipole fields with respect to a common origin. In fact, exploiting the boundary conditions across the surface of the hosting sphere, we get a system of linear nonhomogeneous equations for the amplitudes of the interstitial field that in matrix form reads as

$$\begin{vmatrix} (\mathbf{R})^{-1} + \mathbf{H} & \mathbf{J}_{\leftarrow 0} \\ \mathbf{R}_W \mathbf{J}_{0\leftarrow} & (\mathbf{R}_0)^{-1} \end{vmatrix} \begin{vmatrix} \mathbf{P} \\ \mathbf{P}_0 \end{vmatrix} = \begin{vmatrix} \mathbf{0} \\ \mathbf{W} \end{vmatrix}. \tag{9}$$

The elements of the submatrices that appear in system (9) are explicitly defined in Borghese et al. (1994) and Borghese et al. (2002). Once system (9) has been solved for the amplitudes $P_{\eta\alpha lm}^{(p)}$ and $P_{\eta 0lm}^{(p)}$, the boundary conditions across the surface of the inclusions yield the relation among these amplitudes and the amplitudes $C_{\eta\alpha lm}^{(p)}$ of the multipole fields within the αth inclusion.

2.2. *Description of Field Polarization*

According to equations (4), (7), and (8), the scattered field, the field in the interstitial region, and the fields within the inclusions have the general form

$$\bar{\boldsymbol{E}}(\boldsymbol{r},\ t) = \boldsymbol{E}_g(\boldsymbol{r}) \exp(-i\omega t), \tag{10}$$

where $\boldsymbol{E}_g$ satisfies the vector Helmholtz equation appropriate to the region considered ($g \equiv S$, T, or C). Since $\bar{\boldsymbol{E}}(\boldsymbol{r},\ t)$ is monochromatic, the direction of propagation of the associated electromagnetic energy is given by the time-averaged Poynting vector $\boldsymbol{S} = \mathrm{Re}(\tilde{\boldsymbol{S}})$, where

$$\tilde{\boldsymbol{S}} = \frac{c}{8\pi}\left(\boldsymbol{E}_g \times \boldsymbol{H}_g^*\right) \tag{11}$$

is the complex Poynting vector (Jackson 1975). Both the electric and the magnetic field are orthogonal to $\tilde{\boldsymbol{S}}$. In that sense the electromagnetic waves are *transverse* (Born & Wolf 2002). Nevertheless, the transversality of the field does not imply that at any point the plane swept, for example, by the electric field is orthogonal to the direction of $\boldsymbol{S}$.

This orthogonality is granted for homogeneous plane waves but not for monochromatic waves of general form. The time-averaged $\boldsymbol{S}$ is dependent on $\boldsymbol{r}$ so that both its magnitude and direction change pointwise. In addition, if we write the complex quantity $\boldsymbol{E}_g$ as

$$\boldsymbol{E}_g(\boldsymbol{r}) = \boldsymbol{p}(\boldsymbol{r}) + i\boldsymbol{q}(\boldsymbol{r}), \tag{12}$$

where $\boldsymbol{p}$ and $\boldsymbol{q}$ are real vectors, equation (10) reads

$$\bar{\boldsymbol{E}}(\boldsymbol{r},\ t) = \mathrm{Re}\{[\boldsymbol{p}(\boldsymbol{r}) + i\boldsymbol{q}(\boldsymbol{r})] \exp(-i\omega t)\}. \tag{13}$$

At any given point $\boldsymbol{r} = \boldsymbol{r}_0$, the vectors $\boldsymbol{p}(\boldsymbol{r}_0)$ and $\boldsymbol{q}(\boldsymbol{r}_0)$ define a plane on which $\bar{\boldsymbol{E}}(\boldsymbol{r}_0,\ t)$ varies as a function of time. Since $\bar{\boldsymbol{E}}(\boldsymbol{r}_0,\ t)$ is periodic, the curve described by its tip is closed and is an ellipse. To show this we define a pair of vectors $\boldsymbol{a}(\boldsymbol{r})$ and $\boldsymbol{b}(\boldsymbol{r})$ such that

$$\boldsymbol{p}(\boldsymbol{r}) + i\boldsymbol{q}(\boldsymbol{r}) = \left[\boldsymbol{a}(\boldsymbol{r}) + i\boldsymbol{b}(\boldsymbol{r})\right] \exp(-i\gamma), \tag{14}$$

where γ is a real phase that can be chosen so that $\boldsymbol{a}$ and $\boldsymbol{b}$ are mutually orthogonal. The requirement of orthogonality decrees that

$$\tan 2\gamma = \frac{2\boldsymbol{p}\cdot\boldsymbol{q}}{\boldsymbol{p}^2 - \boldsymbol{q}^2}, \tag{15}$$

and the whole field can be written as

$$\bar{\boldsymbol{E}}(\boldsymbol{r}_0,\ t) = \mathrm{Re}\{[\boldsymbol{a}(\boldsymbol{r}_0) + i\boldsymbol{b}(\boldsymbol{r}_0)] \exp[-i(\omega t - \gamma)]\}. \tag{16}$$

Therefore, by choosing a rectangular coordinate system with origin at $\boldsymbol{r}_0$ and the x- and y-axes along $\boldsymbol{a}$ and $\boldsymbol{b}$, respectively, we have

$$E_x(\boldsymbol{r}_0,\ t) = a\cos(\omega t - \gamma),$$
$$E_y(\boldsymbol{r}_0,\ t) = b\sin(\omega t - \gamma),$$

i.e.,

$$\frac{E_x^2}{a^2} + \frac{E_y^2}{b^2} = 1. \tag{17}$$

Thus, a monochromatic field of general form is elliptically polarized. The ellipse may degenerate into a circle or into a straight line. In the latter case the area of the polarization ellipse

$$A = \pi ab \tag{18}$$

vanishes.

Since the electric field $\boldsymbol{E}_g$, and its complex conjugate $\boldsymbol{E}_g^*$, lie in the plane of the polarization ellipse, the real vector

$$\boldsymbol{V} = i\boldsymbol{E}_g \times \boldsymbol{E}_g^* = i(\boldsymbol{a} + i\boldsymbol{b}) \times (\boldsymbol{a} - i\boldsymbol{b}) = 2\boldsymbol{a} \times \boldsymbol{b} \tag{19}$$

(Carozzi et al. 2000) individuates the normal to that plane, and according to the preceding definition, the electric field rotates counterclockwise with respect to $\boldsymbol{V}$. Moreover, the magnitude of $\boldsymbol{V}$, on account of the orthogonality of $\boldsymbol{a}$ and $\boldsymbol{b}$, is

$$|\boldsymbol{V}| = 2ab = \frac{2}{\pi}A \tag{20}$$

and therefore vanishes for linear polarization (Lindell 1983). When $|\boldsymbol{V}| \neq 0$, then

$$\boldsymbol{V} \times \boldsymbol{S} \neq \boldsymbol{0}. \tag{21}$$

This result implies that the plane of the polarization ellipse is not orthogonal to $\boldsymbol{S}$. Therefore, we assume that the quantity

$$V_s = \boldsymbol{V}\cdot\boldsymbol{S}/|\boldsymbol{S}|, \tag{22}$$

the projection of $\boldsymbol{V}$ along the direction of propagation of the electromagnetic energy, gives the sense of rotation of the field with respect to $\boldsymbol{S}$. Since $\boldsymbol{V}$ and $\boldsymbol{S}$ can never become orthogonal, $V_s = 0$ only for linear polarization ($\boldsymbol{V} = 0$).

The lack of orthogonality of the plane of the polarization ellipse and of the Poynting vector prevents a description of the state of polarization of the field in terms of the well-known Stokes parameters. Actually, for monochromatic fields of general

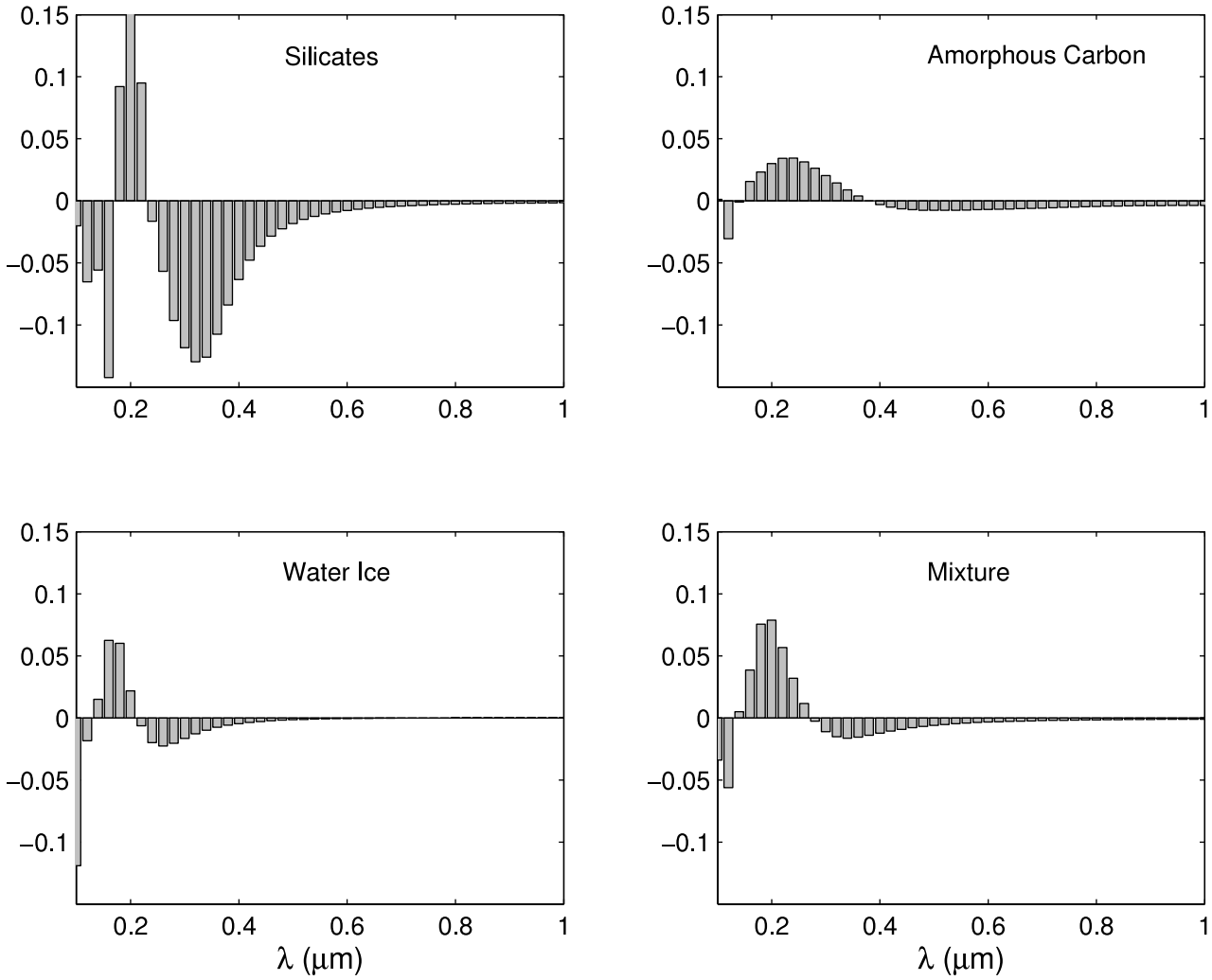

FIG. 2.—V_s calculated at point F of a single cavity inside a sphere of radius $\rho_0 = 100$ nm. The polarization of the incident field is along the x-axis. The interstitial material is indicated in each panel. The volume of the cavity is 40% of the volume of the host sphere. [*See the electronic edition of the Journal for a color version of this figure.*]

form, the most general description of the state of polarization is given by the spectral density tensor that is a Cartesian representation of the coherency dyad (Mishchenko et al. 2004)

$$\mathbf{S}_{d3} = \begin{pmatrix} E_x E_x^* & E_x E_y^* & E_x E_z^* \\ E_y E_x^* & E_y E_y^* & E_y E_z^* \\ E_z E_x^* & E_z E_y^* & E_z E_z^* \end{pmatrix}. \tag{23}$$

The elements of $\mathbf{S}_{d3}$ carry full information on the state of polarization of the field. In particular, the pseudovector associated to $\mathbf{S}_{d3}$ is

$$\boldsymbol{F} = \boldsymbol{E}_g \times \boldsymbol{E}_g^* = -i\boldsymbol{V}. \tag{24}$$

Thus, $\boldsymbol{V}$ is a quantity that stems from the spectral density tensor formalism for the electromagnetic field. Details on the description of the polarization state in terms of the spectral density tensor can be found in Borghese et al. (2005).

3. RESULTS

We approximate a compact grain aggregate with a simple model consisting of a homogeneous sphere embedding a number of empty cavities ($n_\alpha = 1$). We consider host spheres with radii around the value $\rho_0 = 100$ nm taken as a reference. Dust particles of these sizes are efficient in causing interstellar extinction at visual wavelength. We choose four candidates for the interstitial material: (1) silicates (Suh 1999), (2) amorphous carbon (Suh 2000), (3) water ice (Warren 1984), and (4) a Bruggeman mixture (Bohren & Huffman 1983) of 30% silicates, 30% amorphous carbon, and 40% water ice. The Bruggeman mixing rule has been applied to the interstitial material only, whereas cavities have been treated as separate entities. The incident field is assumed to propagate along the z-axis, and the reference plane is chosen to be the x-z plane (Fig. 1). The depolarization of the field has been calculated on the internal surface of the cavity at points F and B in Figure 1 for polarization of the incident wave along the x- and y-axes.

In the next sections we present the results of an extensive grid of models. Calculations have been performed varying the number of inclusions, their positions (both in radius and angle), the sizes of both inclusions and the hosting sphere, and the chemical composition of the interstitial material of the aggregate. Results are discussed in terms of the sign of the quantity V_s, equation (22), which gives the sense of rotation of the field with respect to the direction of propagation of the electromagnetic

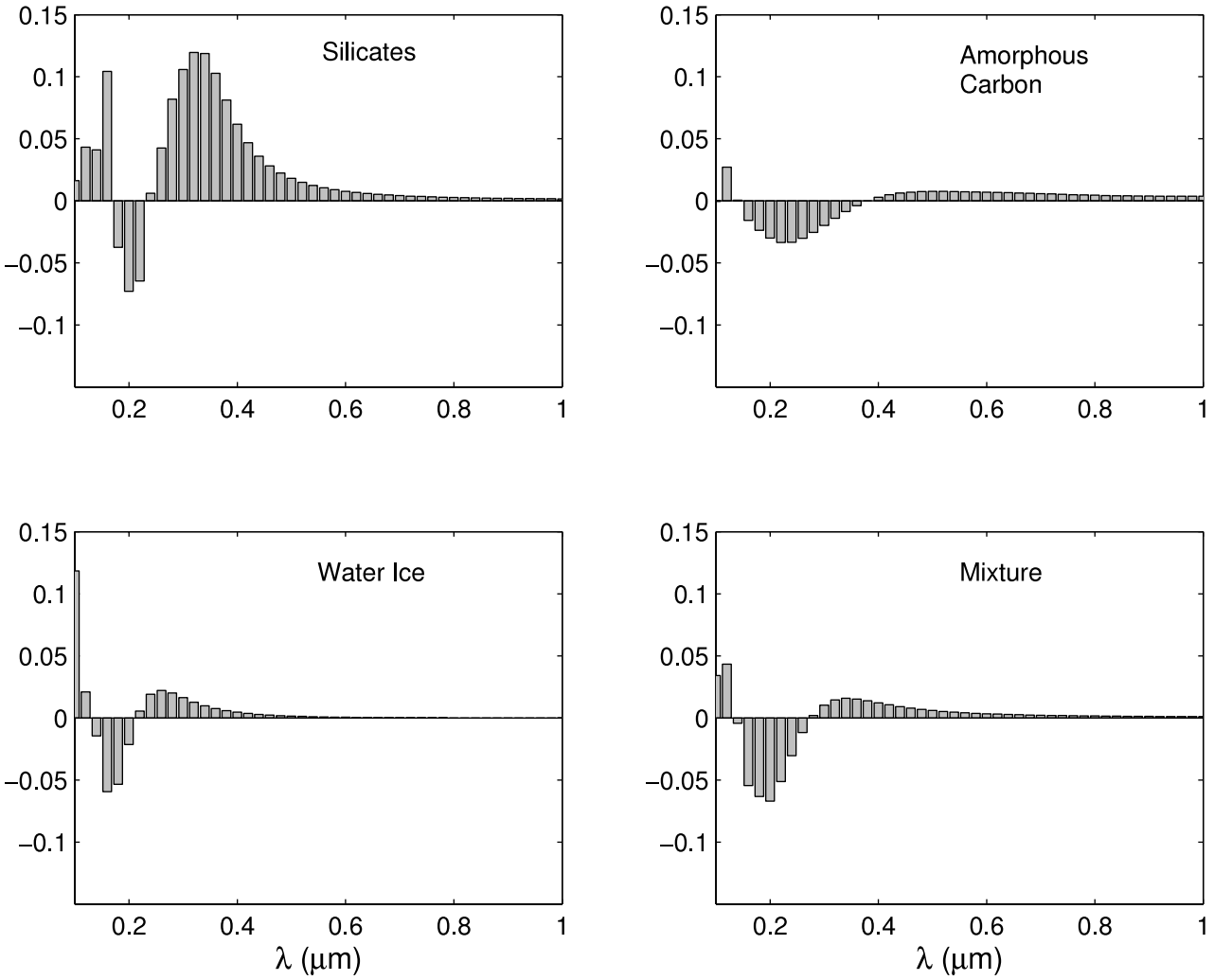

FIG. 3.—Same as Fig. 2, but for polarization of the incident field along the *y*-axis. [*See the electronic edition of the Journal for a color version of this figure.*]

energy and whose magnitude is related to the extent of the depolarization.

3.1. *Single Cavity*

We start our study by using as a reference model a host sphere with radius $\rho_0 = 100$ nm, containing a single spherical inclusion. In the calculations we consider several locations of the cavity. However, results are reported for a cavity tangent to the surface of the host sphere and whose center lies on the radius whose polar angles are $\theta_c = 60^\circ$ and $\phi_c = 30^\circ$. This geometrical configuration produces large depolarization effects. In fact, symmetry considerations show that no depolarization occurs at either point F or point B when the center of the cavity is located on the *z*-axis. In the first part of the modeling exercise, we assess to what extent the occurrence of depolarization depends on the refractive index of the interstitial material and on the polarization of the incident field. We initially assume a cavity with a volume that is 40% of the volume of the host sphere ($\rho_1 = 73.8$ nm). In Figures 2 and 3 we report the quantity V_s calculated at point F for polarizations of the incident field along the *x*- and *y*-axes, respectively, when the interstitial materials are silicate, amorphous carbon, ice, and the Bruggeman mixture. Very similar results are obtained at point B. The maximum value of V_s occurs in the wavelength range 0.1–0.5 μm. The degree of depolarization appears rather small for $\lambda \gtrsim 0.5$ μm, and no depolarization occurs at wavelengths greater than 1 μm. The change in the polarization of the incident field inverts almost exactly the sign of V_s, i.e., the sense of the polarization. Since this is equivalent to a rotation of the grain around the *z*-axis, the sense of polarization turns out to depend strongly on the position of the cavity with respect to the incident field. On the contrary, the depolarization of the field shows little dependence on the choice of the refractive index.

The depolarization of the incident field depends on the dimensions of both the inclusion and the host sphere. Figure 4 shows the results obtained assuming a grain of radius $\rho_0 = 150$ nm and varying the volume of the embedded cavity. The incident field is polarized along the *x*-axis. The maxima of depolarization occur at $\lambda \approx 0.1$–0.5 μm, and the sign of V_s changes when the polarization of the incident field switches from the *x*-axis to the *y*-axis. Similar results are obtained at point B.

For volumes of the embedded cavity larger than the 5% of the volume of the host sphere, the sign of V_s changes twice at approximately 0.2 and 0.3 μm. For smaller inclusions the behavior of V_s is more complicated (cf. Fig. 4).

3.2. *Two Identical Cavities*

The depolarization of the incident field depends certainly on the number of cavities inside the aggregate. In particular, in this section we address the problem of possible cancellation effects due to the mutual position of the internal cavities. To that aim,

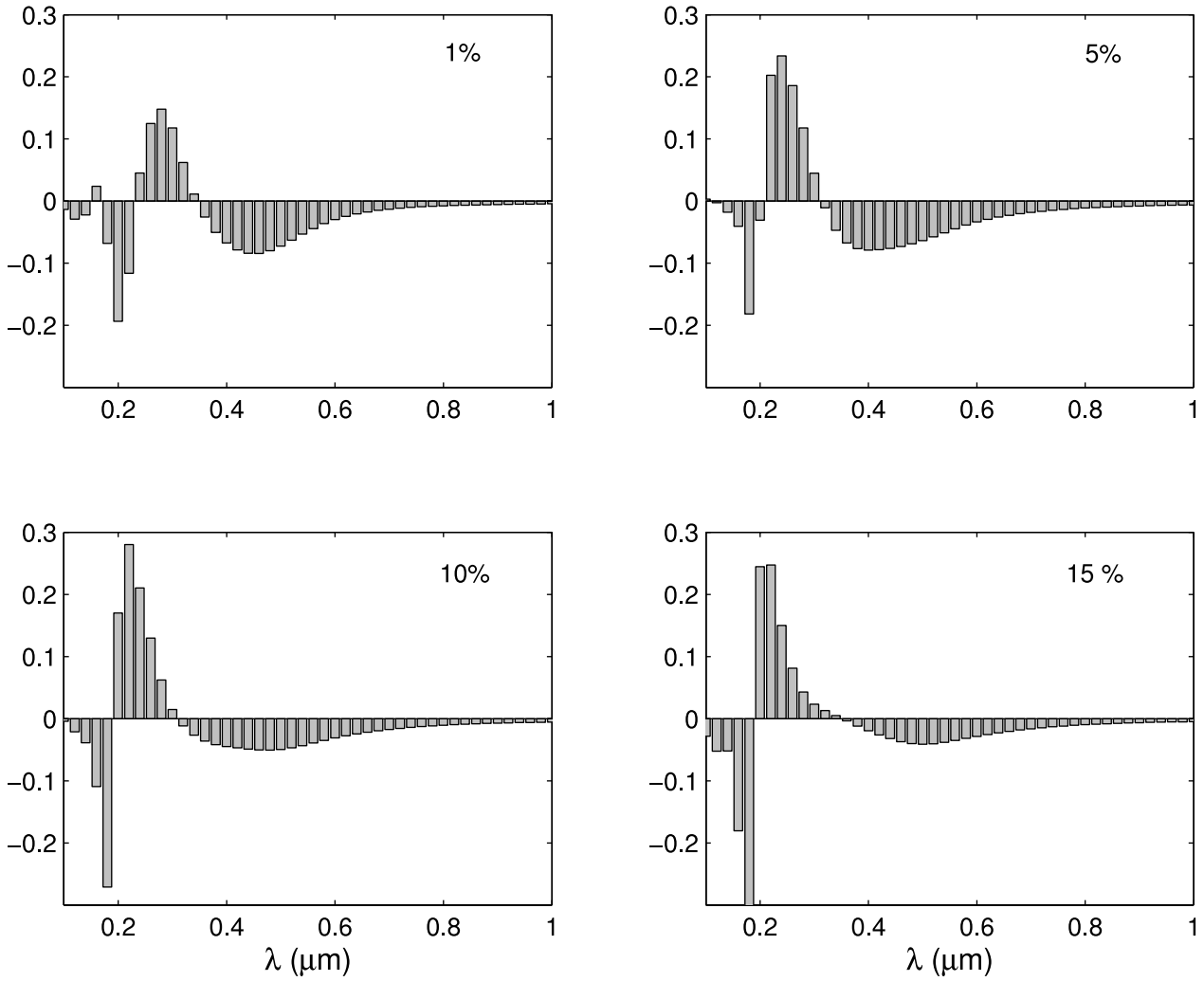

FIG. 4.—V_s calculated at point F of a single cavity of variable volume embedded into a sphere of radius $\rho_0 = 150$ nm. The polarization of the incident field is along the x-axis. The interstitial material is the Bruggeman mixture. The volume of the cavity is indicated in each panel in percent of the volume of the host sphere. [*See the electronic edition of the Journal for a color version of this figure.*]

we consider a model grain formed by a host sphere of 100 nm radius containing two identical empty cavities. We adopt for the interstitial material the same Bruggeman mixture as in § 3.1, in order to simulate grain aggregates of mixed chemical composition. We consider several dispositions for the two cavities. As a representative example, we report the results for the case of two cavities symmetrically placed with respect to the center of the host sphere. The centers of the cavities are located on the diameter whose polar angles are $\theta_c = 66^\circ$ and $\phi_c = 48^\circ$. Our choice of this diameter has no particular significance. The radius of the cavities is $\rho_1 = \rho_2 = 20$ nm so that each of them has a volume of 0.8% of the volume of the host sphere. Cavity 1 has its center located in the upper part of the host sphere. Two mutual distances of the centers are considered: (1) 158 nm, so that the cavities are almost tangent to the surface of the host sphere, and (2) 40 nm. We report V_s calculated at points F of both cavities when the polarization of the incident field is directed along the x-axis (Fig. 5). Results are shown in the wavelength range 0.1–0.5 μm, which is the most relevant to the photochemistry of interstellar ices (Gerakines et al. 1996). Similar results are obtained at point B.

The multiple scattering processes play an important role in determining the behavior of V_s in the two cavities. In fact, in the case of a single cavity, these processes occur between the cavity itself and the internal surface of the host sphere, whereas in the case of two cavities they also occur between the cavities. Moreover, the imaginary part of the refractive index of the interstitial material yields a damping of the strength of the multiple scattering processes. Therefore, when the two cavities are well separated, as in case 1, the behavior of V_s for each cavity is rather similar to the case of a single cavity with a similar volume (cf. Fig. 4, *top left panel*). This happens at both points B and F. When the cavities are in mutual contact, as in case 2, we see that the magnitude of V_s decreases, but this is due to the fact that both cavities are near the center of the host sphere, where symmetry prevents the occurrence of the depolarization. Thus, the high strength of the multiple scattering processes between the cavities is counterbalanced by the general symmetry of the configuration. Note, however, that the depolarization within each cavity is still quite detectable.

3.3. *The General Case*

Our intention in this work is to determine the polarization pattern of the electromagnetic field inside cavities of interstellar dust aggregates and to characterize it in terms of the physical properties of the aggregate. In the preceding sections, we have analyzed the special cases of one and two cavities; here we generalize to a number of cavities as large as $N = 13$. We use as

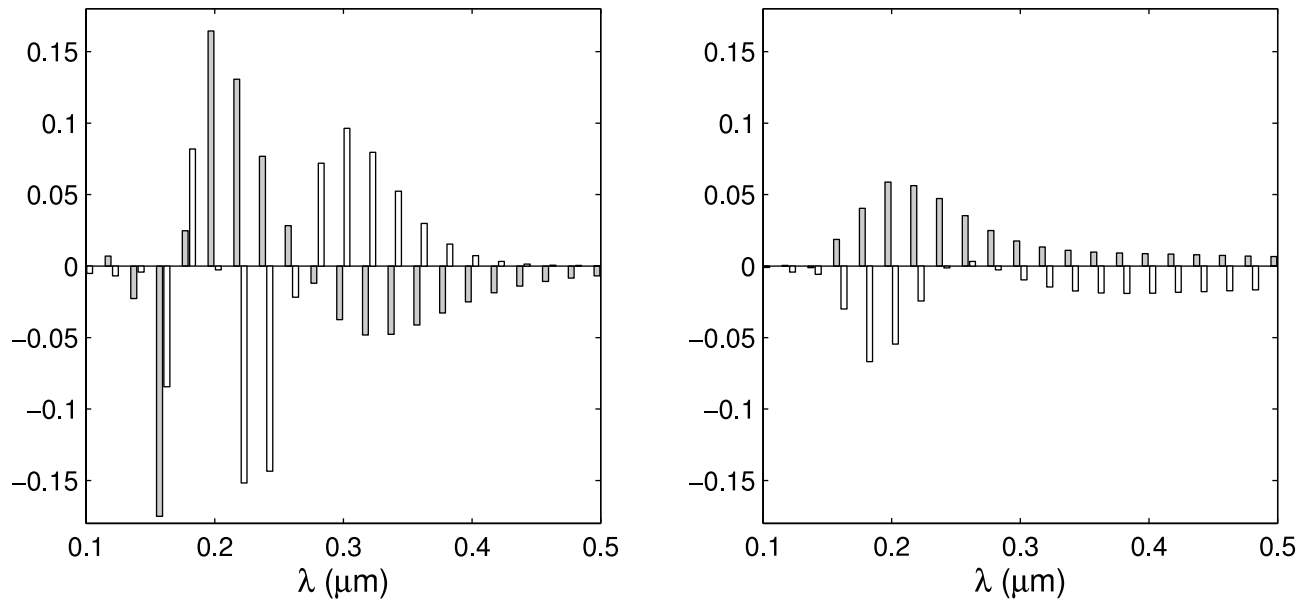

FIG. 5.—V_s calculated at point F for each of the two identical cavities embedded into a sphere of radius $\rho_0 = 100$ nm. The radius of the cavities is $\rho_1 = \rho_2 = 20$ nm, and the distance of their centers is 158 nm (*left*) and 40 nm (*right*). The white bars refer to cavity 1. The polarization of the incident field is along the x-axis. The interstitial material is the Bruggeman mixture. [*See the electronic edition of the Journal for a color version of this figure.*]

interstitial material for the model aggregate the same Bruggeman mixture as in § 3.1.

In presenting the results of numerical computations, we adopt the following strategy: we consider a model aggregate containing a single spherical inclusion and we initially set the radii of the host sphere and the cavity to $\rho_0 = 100$ nm and $\rho_1 = 15$ nm, respectively. The location of the center of the cavity is randomly generated. Results are given at points F of any cavity and for an incident field polarized along the x-axis.

1. We study cooperative effects. To that aim we increase the porosity of grain aggregate, adding in sequence a pair of cavities with radii equal to the first placed cavity, until we reach the final number of $N = 13$ cavities. The location of the centers of the cavities is determined by means of a random number generator; the resulting coordinates are listed in Table 1. The sequence of steps leading to the final configuration is illustrated in Figure 6. We note that some of the inclusions are in contact.

We find that the field undergoes depolarization in the whole set of cavities for any number of cavities included. It is very difficult to find a general trend for the depolarization, as the result depends on the strengths of multiple scattering events that occur among the inclusions as well as among the inclusions and the surface of the host sphere. We show in Figure 7 V_s for three representative cavities (1, 2, and 4) with increasing number of cavities: the persistence of the sign of polarization for inclusion 1, which is relatively isolated from the other cavities, is evident, while in the remaining two inclusions V_s shows variations in both sign and magnitude. Interestingly, but not surprisingly, fluctuations in V_s tend to be damped as the number of inclusions increases. No symmetry considerations apply when the center of a cavity is located on the z-axis. The depolarization pattern for all the inclusions in the final configuration is shown in Figure 8.

TABLE 1
COORDINATES OF THE CENTERS OF THE CAVITIES IN NANOMETERS

n	x	y	z
1	12.102392	−41.166751	2.676656
2	21.329844	21.427363	6.029171
3	30.619547	27.606679	−34.619105
4	−26.950182	−0.313241	13.175339
5	−28.288969	−11.917676	−14.456975
6	−56.500106	−5.155896	11.344851
7	−28.720287	23.705815	−4.711853
8	20.238819	−59.545532	−20.329244
9	−4.082918	25.240899	23.250431
10	−11.017973	−13.366466	−38.943986
11	26.743686	47.711739	−7.380598
12	27.513641	42.776941	−60.313783
13	34.853544	15.799171	32.209947

2. We analyze the role of size parameter of the host sphere using the latest configuration in the simulations discussed in item (1), i.e., considering 13 identical cavities ($\rho_\alpha = 15$ nm). We now vary the radius of the external sphere. We assume three values: $\rho_0 = 100$, 200, and 300 nm. In Figure 9 we show as a representative case V_s for cavity 2. As in the case of a single cavity, the variations in the sign and magnitude of V_s are relevant. The magnitude of V_s decreases rapidly (in the whole set of inclusions) with the increasing size of the host sphere, until no significant field depolarization occurs.

3. The inclusion size parameters may be also important. To study the dependence of the depolarization on the dimension of the inclusions, we set the radius of the host sphere to $\rho_0 = 100$ nm and we decrease the radii of the 13 identical cavities, which means we increase the mutual distance among the surface of the cavities from $\rho_\alpha = 15$ nm (some inclusions in contact) to 10 nm, and 5 nm. The increase in the distance among the surface of the cavities yields a decrease in the strength of the multiple scattering processes. As a result, the pattern of the depolarization can undergo dramatic changes. This can be seen in Figure 10, where we report V_s for cavities 1 (*top panels*) and 13 (*bottom panels*) for decreasing values of their radii. In general, we can state that the depolarization pattern persists for the most part of the inclusions. Some inclusions, which in the case of the largest size showed a constant sign of V_s, present alternations in the sign of this latter

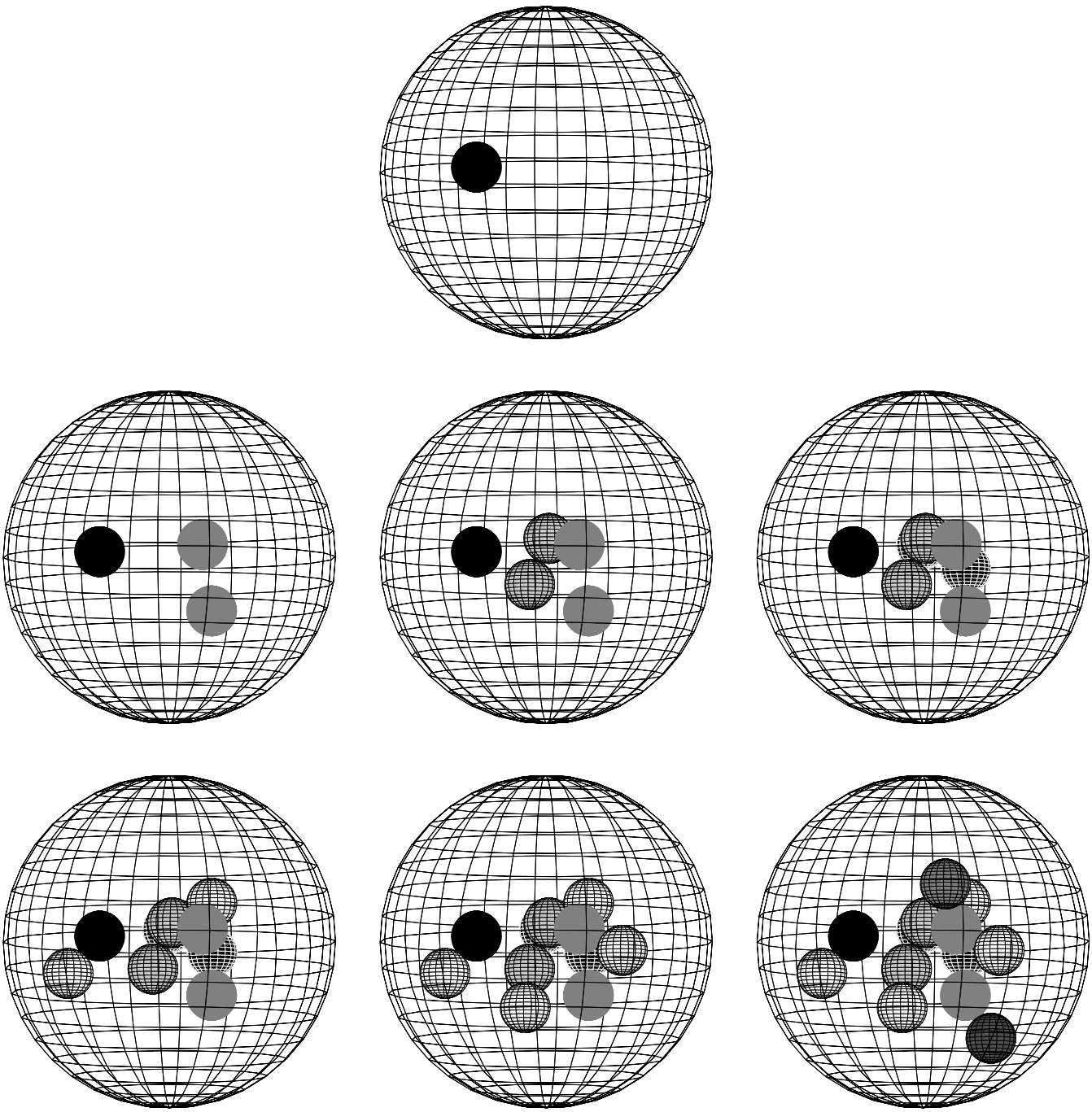

FIG. 6.—Sequence of the configurations attained by adding pairs of cavities with random choice of their position. The coordinates of all cavities are reported in Fig. 1. [*See the electronic edition of the Journal for a color version of this figure.*]

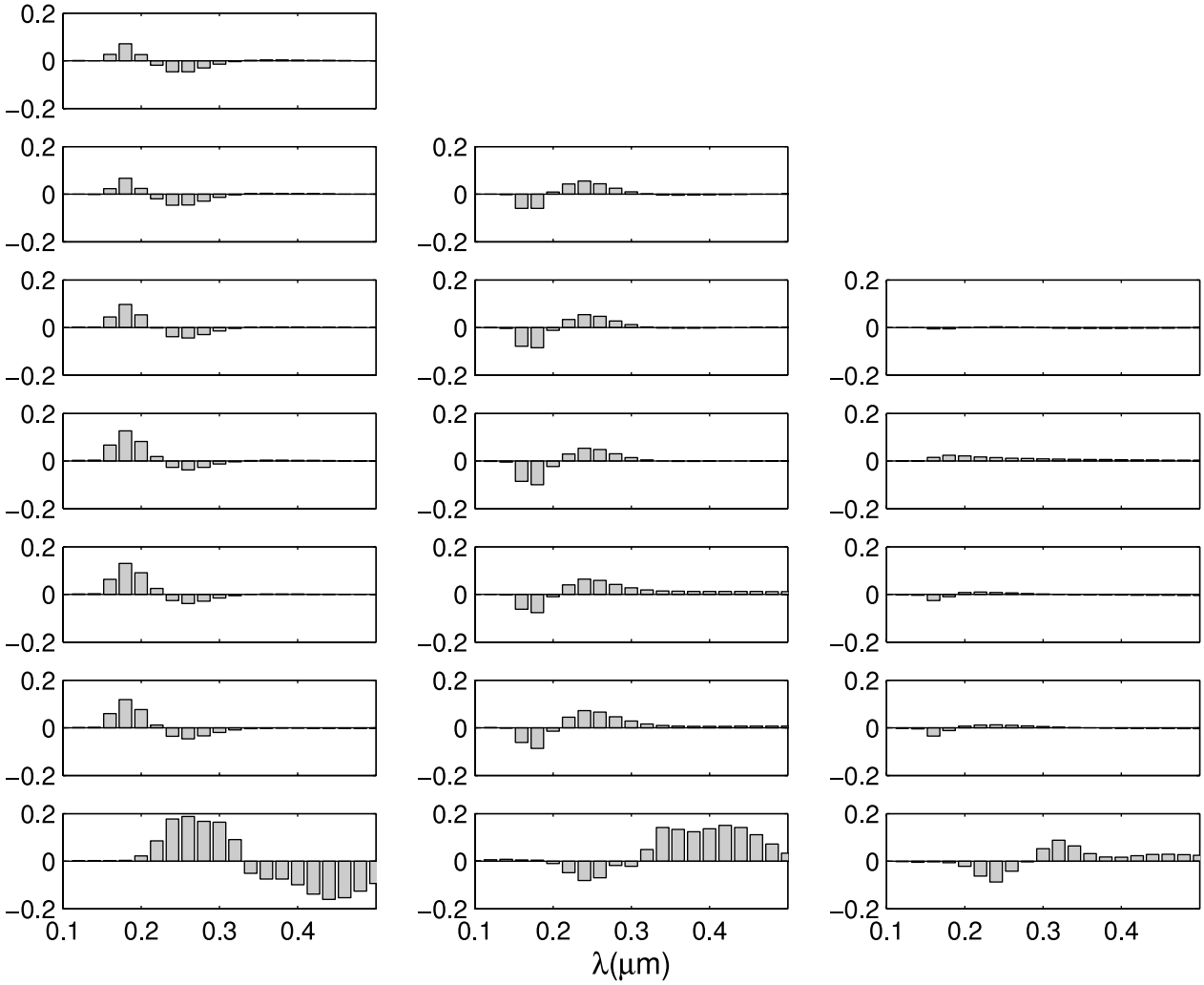

FIG. 7.—Sequence of the values of V_s for cavities 1 (*left*), 2 (*middle*), and 4 (*right*) with increasing numbers of the cavities. [*See the electronic edition of the Journal for a color version of this figure.*]

quantity as their sizes decrease, i.e., as cooperative effects disappear and they act as independent entities.

Random accretion of particles having a size distribution should produce grains with internal voids of sizes comparable to those of the coagulating particles. Thus, we introduce a further generalization, letting the 13 inclusions have a size distribution. We adopt a Gaussian distribution centered at $\overline{\rho} = 10.62$ nm with variance $\Delta\rho = 2.89 \times 10^{-2}$ nm. The locations of the centers of the cavities are also in this case randomly generated. The obtained configuration is shown in Figure 11, while in Figure 12 we report the depolarization pattern for the whole set of 13 cavities. The mutual locations of the inclusions and their sizes are such that cavities are relatively distant from each other. As in the case of small identical inclusions ($\rho_\alpha = 5$ nm), treated in case 3, the cavities may be considered as independent.

By studying the behavior of grain particles in a gas flow simulating a protoplanetary disk, Nakamura & Hidaka (1998) were able to show that, even in a subsonic regime, grains preferentially assume an aligned configuration. Alignment of grain particles is also favored by the exchange of angular momentum between the incident radiation and the particles (Draine & Weingartner 1996). This is also true for nonhomogeneous spheres, for example, for spheres including cavities. Since the aggregates in the protoplanetary disk are aligned, they must share the same geometrical asymmetry: the denser part leading and the more porous one following. To simulate to some extent an irregular geometry, we shift the inclusion cluster of the final configuration shown in Figure 6 along the x-axis toward the surface of the host sphere (Fig. 13). As evident in Figure 14, the depolarization effect is persistent, although variations in both sign and magnitude of V_s with respect to the case illustrated in Figure 8 are present due to interaction with the external surface of the model aggregate.

The numerical simulations described above show that field depolarization occurs in all examined cases and in the whole set of inclusions. The structure of the depolarized field in a cavity is dependent on the number, location, and sizes of the cavities. It depends strongly on the size of the host sphere. Moreover, as the imaginary part of the refractive index of the interstitial material yields a damping of the multiple scattering processes, in some instances neighboring cavities behave as if they were independent. Some cavities show a persistence in both sign and magnitude of V_s, while others do not.

4. CONCLUSIONS

This is the second of a series of papers devoted to the study of the properties of the electromagnetic field within cavities in interstellar grain aggregates. In the first paper we described the

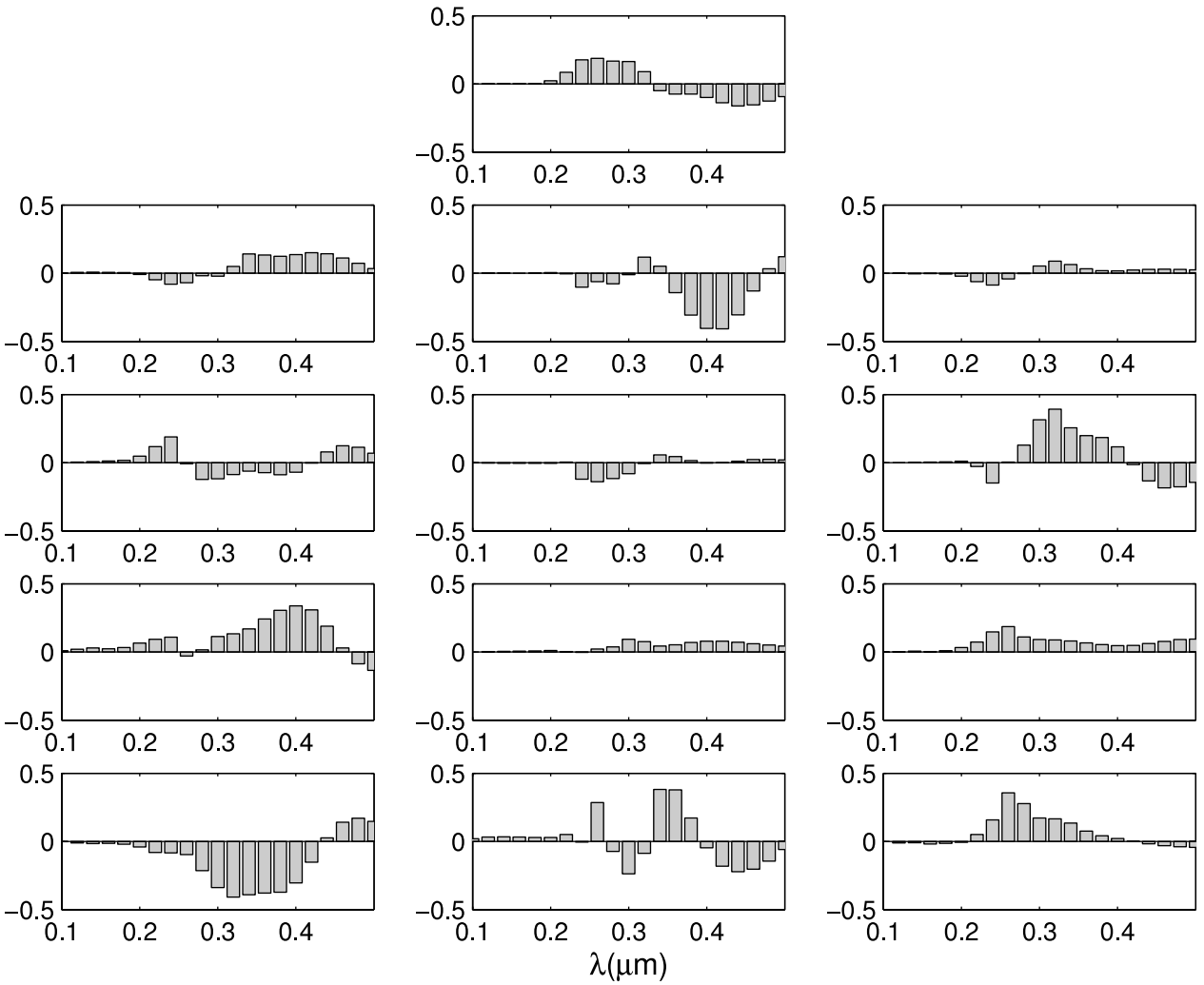

FIG. 8.—Values of V_s for the final configuration of 13 cavities. [*See the electronic edition of the Journal for a color version of this figure.*]

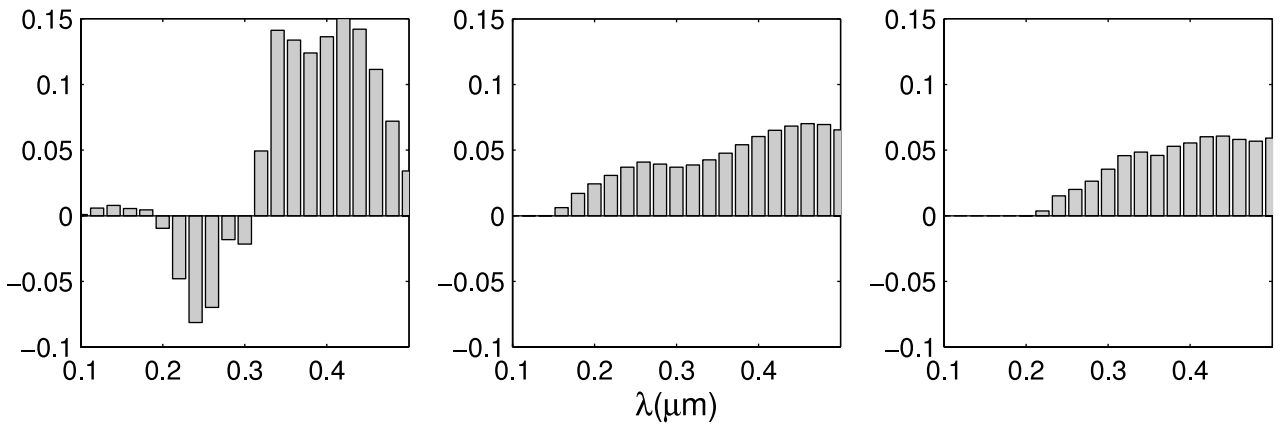

FIG. 9.—Values of V_s for cavity 2 for three different radii of the host sphere: 100 nm (*left*), 200 nm (*middle*), and 300 nm (*right*). [*See the electronic edition of the Journal for a color version of this figure.*]

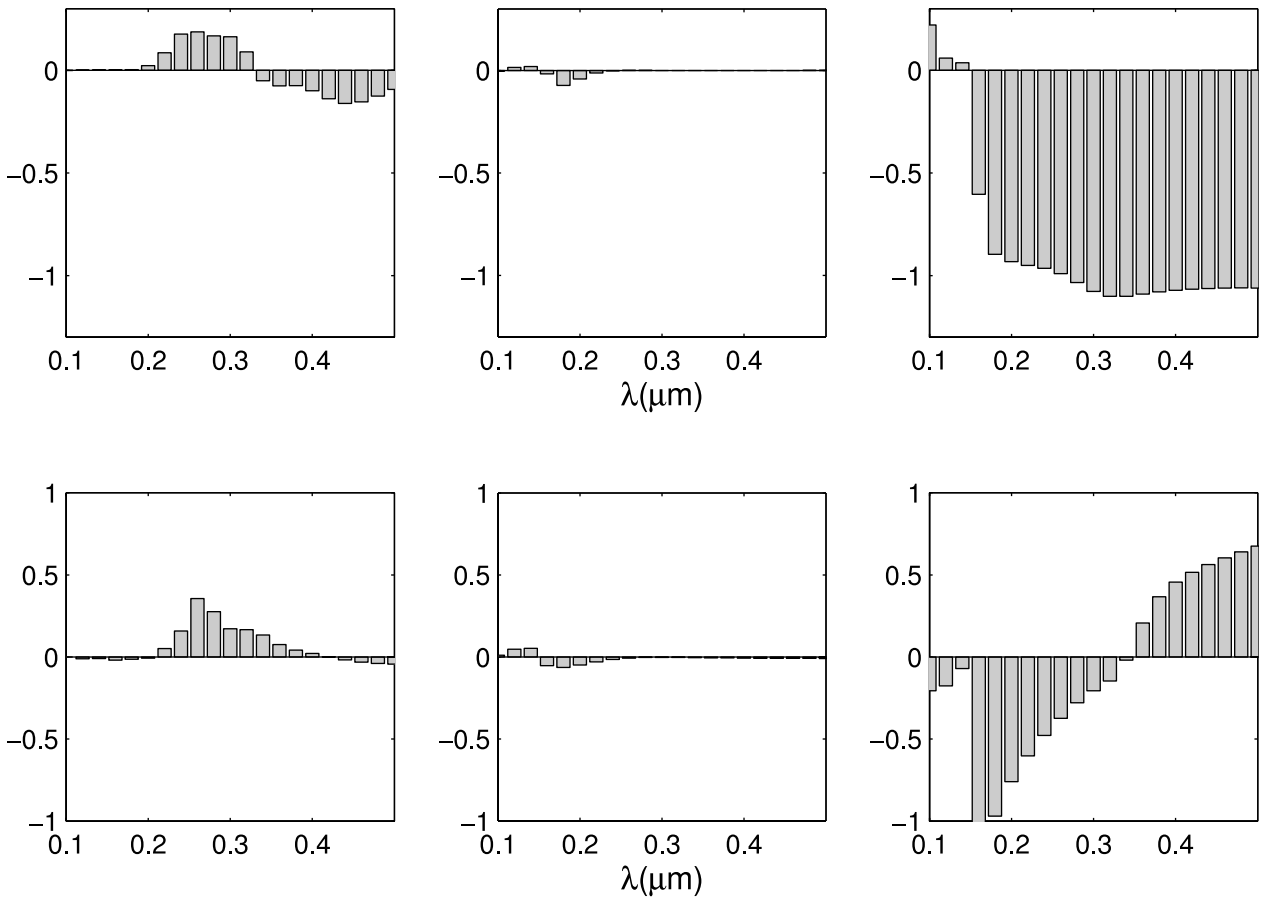

FIG. 10.—Values of V_s for cavities 1 (*top*) and 13 (*bottom*) for three different radii of the cavities: 15 nm (*left*), 10 nm (*middle*), and 5 nm (*right*). [*See the electronic edition of the Journal for a color version of this figure.*]

energy density distribution; here we focus on the polarization pattern of the field in the UV, which is the spectral range more relevant for the interstellar photochemistry. To that end we modeled grain aggregates as homogeneous spheres containing a number of spherical voids.

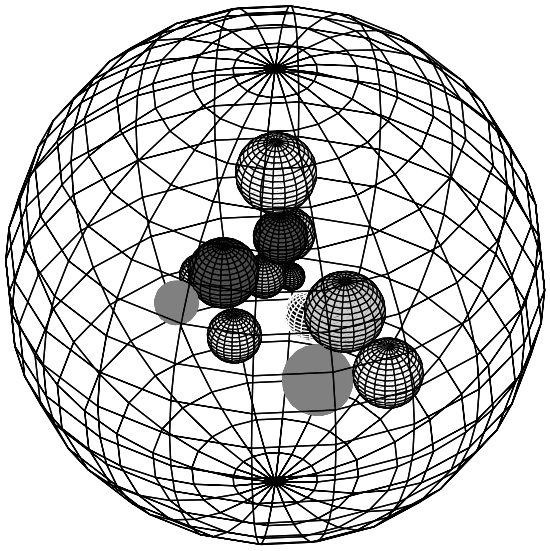

FIG. 11.—Sketch of the configuration of 13 cavities with Gaussian distribution of their radii. [*See the electronic edition of the Journal for a color version of this figure.*]

We start from the consideration that the state of polarization of the field within the cavities cannot be described in terms of the well-known Stokes parameters: the plane of the polarization ellipse is, in fact, not orthogonal to the direction of propagation of the electromagnetic energy that is given by the direction of the Poynting vector $\boldsymbol{S}$. Consequently, the state of polarization of the field has been described by introducing the vector $\boldsymbol{V}$ (eq. [22]), which can be derived from the tensor formalism of the electromagnetic field. The projection of $\boldsymbol{V}$ on $\boldsymbol{S}$ gives the sense of rotation of the field with respect to the direction of propagation of the electromagnetic energy and is thus a suitable description of the polarization of the field.

Our main result is that when a linearly polarized electromagnetic plane wave hits the model grain, the field inside the cavities is elliptically polarized in all the cases that we discussed in the preceding sections. This depolarization effect is of purely geometrical nature: it does not depend on the material of the grain but only on the existence of an asymmetric interface between regions of different refractive indexes. For the range of sizes that are relevant for interstellar grains, the depolarization of the field occurs only in the UV. This means that the magnitude of V_S does not vanish except at particular wavelengths that mark the inversions of the sense of rotation of the field. The position of the inversion wavelengths is fine-tuned by the sizes of the cavities and the host sphere. Anyway, the depolarization effect tends to disappear when the size of the host sphere increases with respect to the size of the inclusions. Since asymmetric photolysis by UV circularly polarized light induces an enantiomeric selection in chiral molecules (Flores et al. 1977), these results might be

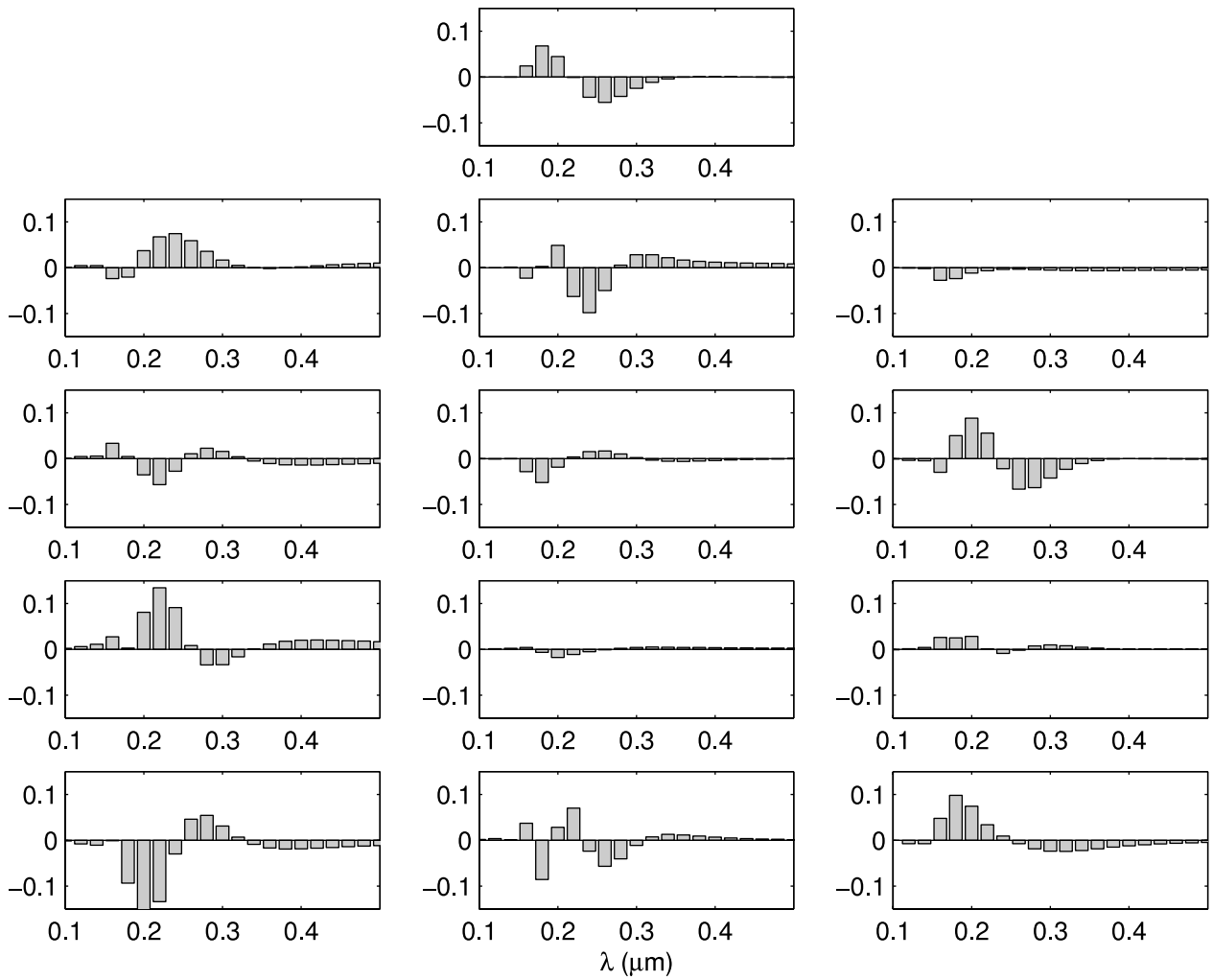

FIG. 12.—Values of V_s for the configuration of 13 cavities shown in Fig. 11. [*See the electronic edition of the Journal for a color version of this figure.*]

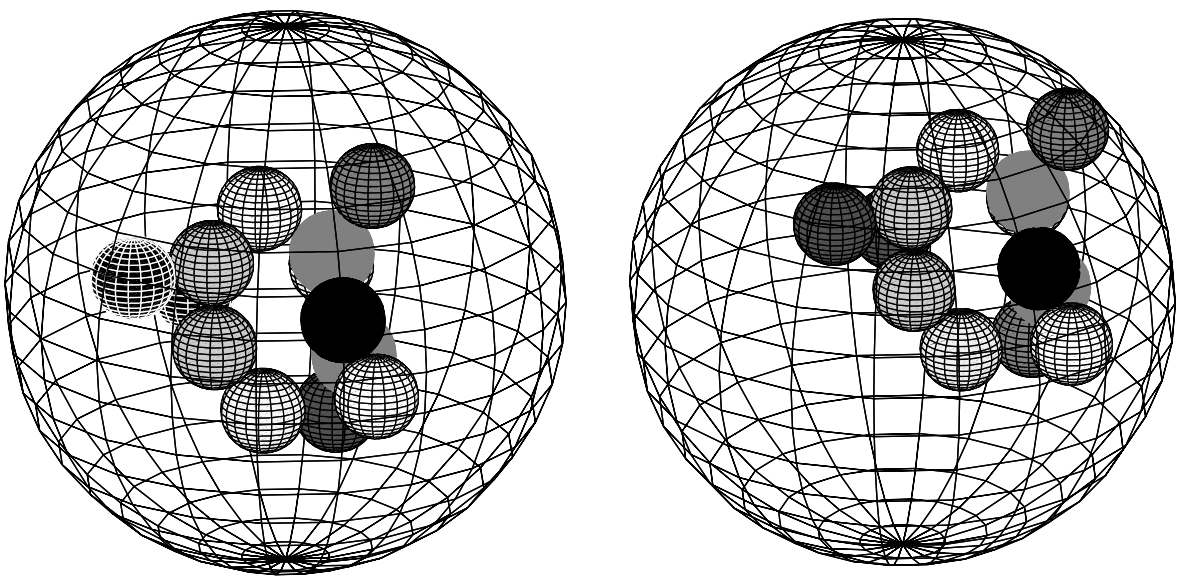

FIG. 13.—Sketch of the configuration of 13 cavities of Fig. 6 (*left*) and of the same configuration rigidly shifted along the *x*-axis (*right*). Note that the point of view has been changed with respect to Fig. 6. [*See the electronic edition of the Journal for a color version of this figure.*]

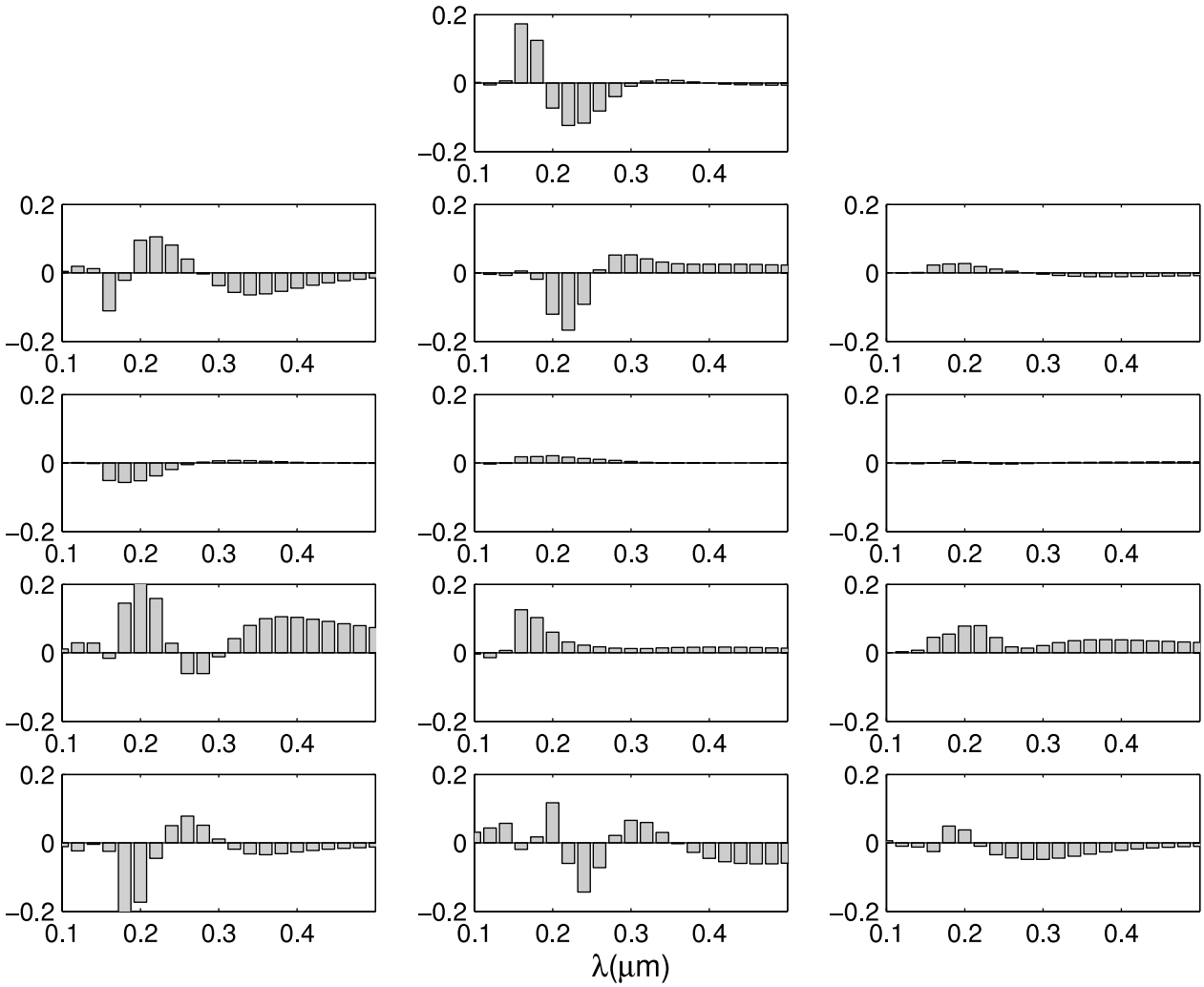

FIG. 14.—Values of V_s for the 13 cavities in the shifted configuration (Fig. 13, *right*). [*See the electronic edition of the Journal for a color version of this figure.*]

important for highlighting the mechanism leading to amino acid asymmetries observed in carbonaceous meteorites (Cronin & Pizzarello 1997).

Ultimately, in spite of the difficulty of finding general recipes to foresee the behavior of the depolarization pattern, we can state, as a general result, that V_s is larger and with a persistent sign when a cavity is comparatively isolated and near the surface of the host sphere. Finally, our calculation produced such a large amount of data that a choice of what to show was in order. Anyway, as maximum care has been exercised in generating the positions of the centers of the cavities, we can claim the generality of our results; i.e., our choice of a simple model for the aggregate has no influence on the behavior of the field inside the cavities. We will present the results of a more general model of grain aggregates, viz., real fluffy aggregates of the kind described by Iatì et al. (2004), in the next paper of the series.

REFERENCES

Bohren, C. F., & Huffman, D. R. 1983, Absorption and Scattering of Light by Small Particles (New York: Wiley)

Borghese, F., Denti, P., & Saija, R. 1994, Appl. Opt, 33, 484

———. 2002, Scattering by Model Nonspherical Particles (Heildelberg: Springer)

Borghese, F., Denti, P., Saija, R., & Cecchi-Pestellini, C. 2005, in J. Phys. Conf. Ser. 6, Light, Dust, and Chemical Evolution, ed. R. Saija & C. Cecchi-Pestellini (London: IOP), 59

Borghese, F., Denti, P., Saija, R., & Sindoni, O. I. 1992, J. Opt. Soc. Am. A, 9, 1327

Borghese, F., Denti, P., Toscano, G., & Sindoni, O. I. 1980, J. Math. Phys., 21, 2754

Born, M., & Wolf, E. 2002, Principles of Optics (7th ed.; Cambridge: Cambridge Univ. Press)

Bradley, J. P., et al. 2005, Science, 307, 244

———. 1999, Science, 285, 1716

Carozzi, T., Karlsson, R., & Bergman, J. 2000, Phys. Rev. E, 61, 2024

Cecchi-Pestellini, C., Saija, R., Iatí, M. A., Giusto, A., Borghese, F., Denti, P., & Aiello, S. 2005, ApJ, 624, 233

Cecchi-Pestellini, C., Scappini, F., Saija, R., Iatí, M. A., Giusto, A., Aiello, S., Borghese, F., & Denti, P. 2004, Int. J. Astrobiology, 3, 287

Cronin, J. R., & Pizzarello, S., 1997, Science, 275, 951

Dominik, C., & Tielens, A. G. G. M. 1997, ApJ, 480, 647

Draine, B. T. 1985, in Protostars and Planets II, ed. D. C. Black & M. S. Mathews (Tucson: Univ. Arizona Press), 621

———. 2003, ARA&A, 41, 241

Draine, B. T., & Weingartner, J. C. 1996, ApJ, 470, 551

Duley, W. W. 2000, MNRAS, 319, 791

Flores, J. I., Bonner, W. A., & Massey, G. A. 1977, J. Am. Chem. Soc., 99, 3622

Fucile, E., Borghese, F., Denti, P., Saija, R., & Sindoni, O. I. 1997, IEEE Trans. Antennas Propag., 45, 868

Gerakines, P. A., Schutte, W. A., & Ehrenfreund, P. 1996, A&A, 312, 289

Gibb, E. L., Whittet, D. C. B., Boogert, A. C. A., & Tielens, A. G. G. M. 2004, ApJS, 151, 35

Iatì, M. A., Giusto, A., Saija, R., Borghese, F., Denti, P., Cecchi-Pestellini, C., & Aiello, S. 2004, ApJ, 615, 286

Jackson, J. D. 1975, Classical Electrodynamics (New York: Wiley)
Jorissen, A., & Cerf, C. 2002, Origins of Life Evol. Biosphere, 32, 129
Lindell, I. V. 1983, Int. J. Electrical Eng. Educ., 20, 33
Lissauer, J. J. 1993, ARA&A, 31, 129
Malloci, G., Mulas, G., & Benvenuti, P. 2004, A&A, 420, 809
Micela, G. 2002, in ASP Conf. Ser. 269, The Evolving Sun and Its Influence on Planetary Environments, ed. B. Montesinos, A. Gimenez, & E. F. Guina (San Francisco: ASP), 107
Mishchenko, M. I., Hovenier, J. W., & Mackowski, D. W. 2004, J. Opt. Soc. Am. A, 21, 71
Nakamura, R., & Hidaka, Y. 1998, A&A, 340, 329
Rose, M. E. 1957, Elementary Theory of Angular Momentum (New York: Wiley)
Suh, K.-W. 1999, MNRAS, 304, 389
———. 2000, MNRAS, 315, 740
Warren, S. G. 1984, Appl. Opt., 23, 1206
Whittet, D. C.B, 1992, Dust in the Galactic Environment (London: IOP)
Wooden, D. H., Harker, D. E., Woodward, C. E., Butner, H. M., Koike, C., Witteborn, F. C., & McMurtry, C. W. 1999, ApJ, 517, 1034